Materials Science & Engineering A 662 (2016) 241–250

Contents lists available at ScienceDirect

Materials Science & Engineering A

journal homepage: www.elsevier.com/locate/msea

Microstructure evolution and mechanical properties of directionally solidified Mg-*x*Gd (x=0.8, 1.5, and 2.5) alloys

Shifeng Luo [a], Guangyu Yang [a,*], Shaojun Liu [a], Jiahe Wang [a], Jiehua Li [b,*], Wanqi Jie [a]

[a] State Key Laboratory of Solidification Processing, Northwestern Polytechnical University, No. 127 Youyi Western Road, Xi'an 710072, PR China
[b] Chair of Casting Research, Montanuniversität Leoben, Franz-Josef-Straße 18, Leoben 8700, Austria

ARTICLE INFO

Article history:
Received 17 January 2016
Received in revised form
12 March 2016
Accepted 14 March 2016
Available online 16 March 2016

Keywords:
Mg-Gd alloys
Directional solidification
Microstructures
Cellular spacing
Mechanical properties

ABSTRACT

The microstructure evolution and mechanical properties of directionally solidified Mg-0.60, 1.38 and 2.35 wt% Gd alloys were investigated as a function of temperature gradients (G), growth rates (V), cooling rates (R) and solute (Gd) contents. A typical cellular microstructure with varied morphologies was observed in three different Mg-Gd alloys under steady states with three different G (20, 25, and 30 K/mm) at the fixed V (10 μm/s) or with different V (10–200 μm/s) at the fixed G (30 K/mm). The formation of cellular microstructure can be attributed to the combined effects of the lower solute content and the higher interfacial tension. The cellular spacing (λ) decreases not only with increasing G or V, but also with increasing Gd content for the fixed G and V. The measured λ values are in good agreement with Trivedi model and the previous experimental results. Meanwhile, the ultimate tensile strength of directionally solidified Mg-Gd alloys decreases with increasing λ, but it increases with increasing cooling rates. Furthermore, the relationship between the ultimate tensile strength, structure parameter and cooling rate was also discussed and compared with the previous experimental results.

1. Introduction

Magnesium alloys, as the lightest metal structural materials in industrial application, have been attracted more and more attention in aerospace and automotive industries [1,2]. However, a barrier to their wider application of commercial Mg alloys, such as AZ91D and ZK51, is their relatively poor performance, in particular at elevated temperatures [3,4]. It is well-accepted that the addition of rare element (RE, e.g. Gd) into Mg alloy is promising to improve the alloy performance at elevated temperatures [5,6]. Indeed, to date, alloying and subsequent solution and ageing treatment are still one of the most important ways to enhance mechanical properties of Mg-Gd based alloy [7–13]. It is worth nothing that increasing Gd content would improve mechanical properties, however, the density and the costs are also increased [11–13]. A good balance between performance and density as well as costs should be taken into consideration.

In another way, Mg alloy performance can be also improved by the directional solidification technique. Pailwal et al. [14] investigated the comprehensive microstructural evolution of Mg-3, 6, and 9 wt% Al alloys by using directional solidification and other solidification techniques and built a solidification map based on the experimental data and the solidification model. Liu et al. [15] investigated the microstructure and mechanical properties of directionally solidified Mg-3.0Nd-1.5Gd alloy. A significant improvement of ultimate tensile strength (UTS) (59% higher) and elongation (112% higher) was obtained when comparing with the non-directionally solidified alloy under the same cooling rates. It is, therefore, very interesting to investigate the effect of directional solidification technique on the microstructure evolution and mechanical properties of Mg-Gd binary alloys.

In this paper, the microstructure evolution and mechanical properties of directionally solidified Mg-*x*Gd (x=0.8, 1.5, and 2.5) alloys were investigated as a function of temperature gradients (G), growth rates (V), cooling rates (R) and solute (C_0) contents. Meanwhile, the correlation between ultimate tensile strength, structure parameter and cooling rate is also discussed.

2. Experimental procedures

2.1. Alloy preparation

The alloy ingots with nominal compositions of Mg-0.8 Gd, Mg-1.5 Gd, and Mg-2.5 Gd (wt%, used throughout the paper unless noted) were melted from pure Mg (99.98) and Mg-28 Gd master alloy in an electrical-resistance furnace under the protection of anti-oxidizing (RJ-4). The melting alloys were homogenized at

* Corresponding authors.
E-mail addresses: ygy@nwpu.edu.cn (G. Yang), jie-hua.li@hotmail.com (J. Li).

http://dx.doi.org/10.1016/j.msea.2016.03.065
0921-5093/

Table 1
Chemical composition of Mg-Gd alloys.

Nominal alloys	Composition (wt%)	
	Gd	Mg
Mg-0.8 Gd	0.60	Bal.
Mg-1.5 Gd	1.38	Bal.
Mg-2.5 Gd	2.35	Bal.

780 °C for 20 min followed by casting into a test bar (Φ 10 × 150 mm) in a Fe mould at 740 °C. The test bars were further processed into the samples of Φ 7.8 × 90 mm for subsequent directional solidification experiments. The composition of the alloys were determined through inductively coupled plasma atomic emission spectrum (ICP-AES) apparatus and listed in Table 1.

2.2. Directional solidification experiments

Directional solidification experiments were performed in a high-temperature gradient Bridgman-type directional furnace with a graphite heater and the quenching system of water-cooled Ga-In-Sn liquid metals. The prepared sample (Φ 7.8 × 90 mm) was loaded in a special stainless tube crucible with an outer diameter (OD) of 10 mm, an inner diameter (ID) of 8 mm and a length of 120 mm. The ends of tube crucibles were sealed. A special sulfur dioxide (SO_2) generator was inserted into the top of the crucible, which was designed to prevent the oxidation of the experimental alloy [15]. The crucible was put in the vacuum furnace with the graphite heater, pumped down to 0.01 mbar, backfilled with high-purity Ar gas, and then heated to 800 °C for 30 min. After stabilizing the thermal conditions in the furnace under an argon atmosphere, the specimen was grown by means of different speed synchronous motors. Specimens were solidified under steady state conditions with different temperature gradients (G=20, 25 and 30 K/mm) at the constant growth rate (V=10 μm/s) or with different growth rates (V=10–200 μm/s) under the constant temperature gradient (G=30 K/mm). The samples were directionally solidified about 40–50 mm, and then quenched rapidly into the Ga-In-Sn liquid metals. In this paper, the growth rate is substituted for the withdrawal rate. They can be regarded to be identic when the solidification process is in the steady state after a short initial transient zone during directional solidification process.

2.3. Sample characterization

The microstructural evolution of the directionally solidified alloy samples was characterized from the longitudinal and transverse sections, which are believed to be located at about 5 mm below the quenched solid-liquid interface. The solidification

Table 2
The experimental results and the relationships between the cellular spacing and solidification parameters for Mg-Gd alloys.

C_0 (Mg-wt% Gd)	G (K/mm)	V (μm/s)	$R(R=GV)$ (K/s)	λ (μm)	Relationships	Correlation coefficients (r)
0.60	20	10	0.20	73	$\lambda=109.72V^{-0.2615}$	−0.994
	25	10	0.25	66	$\lambda=275.25G^{-0.4432}$	−0.999
	30	10	0.30	61	$\lambda=44.75R^{-0.2784}$	−0.995
	30	40	1.20	40		
	30	100	3.00	34		
	30	150	4.50	30		
	30	200	6.00	27		
1.38	20	10	0.20	85	$\lambda=135.74V^{-0.2598}$	−0.987
	25	10	0.25	80	$\lambda=213.96G^{-0.3073}$	−0.994
	30	10	0.30	75	$\lambda=54.96R^{-0.2656}$	−0.994
	30	40	1.20	50		
	30	100	3.00	44		
	30	150	4.50	37		
	30	200	6.00	33		
2.35	20	10	0.20	112	$\lambda=159.19V^{-0.2763}$	−0.992
	25	10	0.25	97	$\lambda=935.58G^{-0.7071}$	−0.997
	30	10	0.30	84	$\lambda=62.83R^{-0.3093}$	−0.990
	30	40	1.20	57		
	30	100	3.00	45		
	30	150	4.50	42		
	30	200	6.00	35		

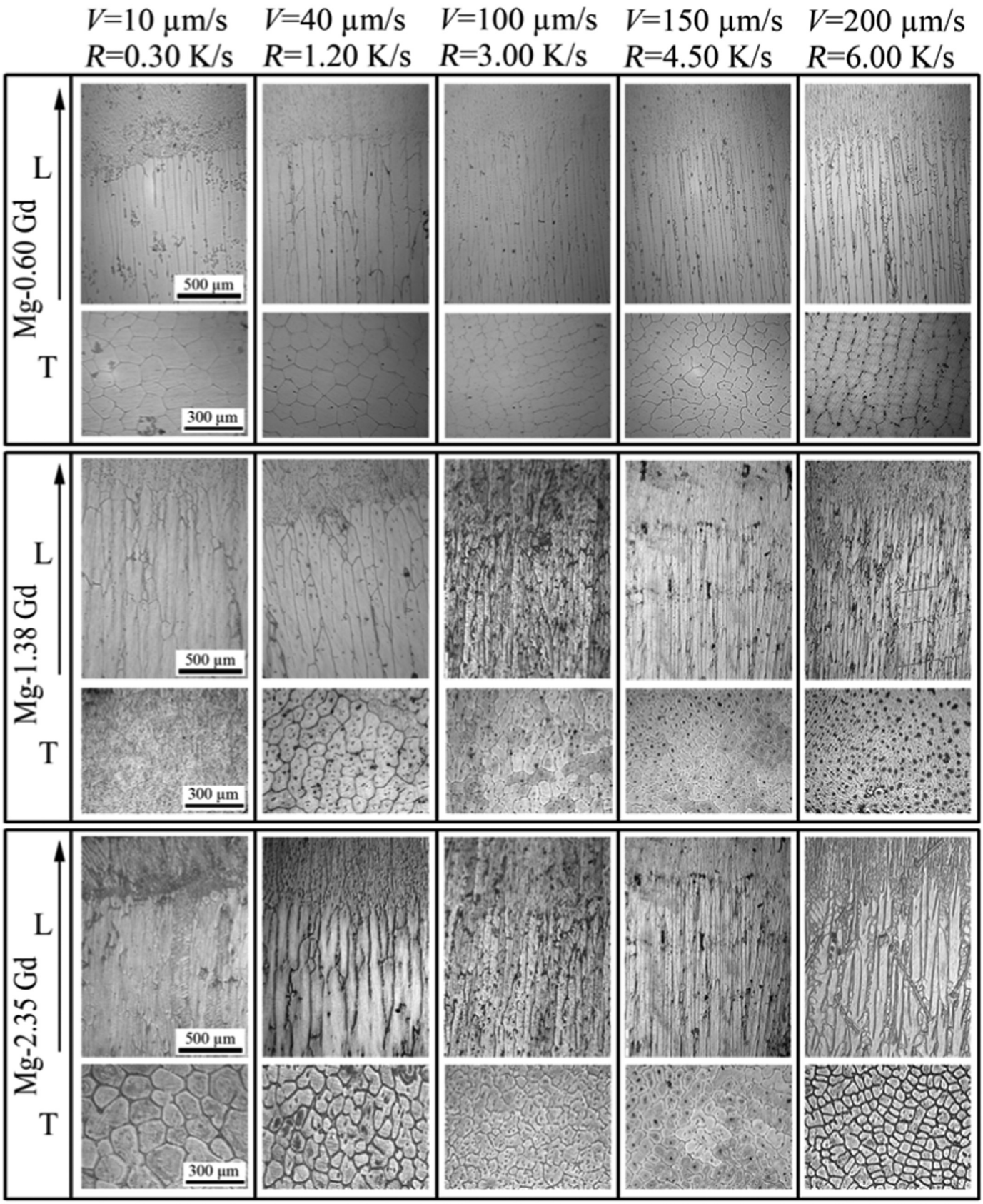

Fig. 1. OM images of directionally solidified Mg-Gd experimental alloys under $G=30$ K/mm at different growth rates. L and T represent the longitudinal and the transverse section of samples, respectively.

microstructures were examined by using Olympus PM-G3 type optical microscope (OM). The cellular spacing (λ) was measured from the OM images of the solidified samples using the area counting method. In this method, the average cellular spacing values were calculated using an Eq. (1):

$$\lambda = \frac{B}{M}\left(\frac{A}{N}\right)^{0.5} \quad (1)$$

where B (1.075 for hexagonal structures) is the correction factor, M is the magnification factor, A is the total specimen cross-section area and N is the number of cell on the cross-section. λ values were measured on the cross-section with at least five different regions for each specimen. The experimental results and the relationship between λ and solidification parameters for the experimental alloys are given in Table 2.

Tensile test was carried out by using a Zwick 150 type universal tensile testing machine at a strain rate of 0.007/s at room temperature. The test specimen was rectangular in shape with 20 mm in length, 5 mm in width, and 2 mm in height. At least three specimens were tested at each condition to ensure the reproducibility of the data.

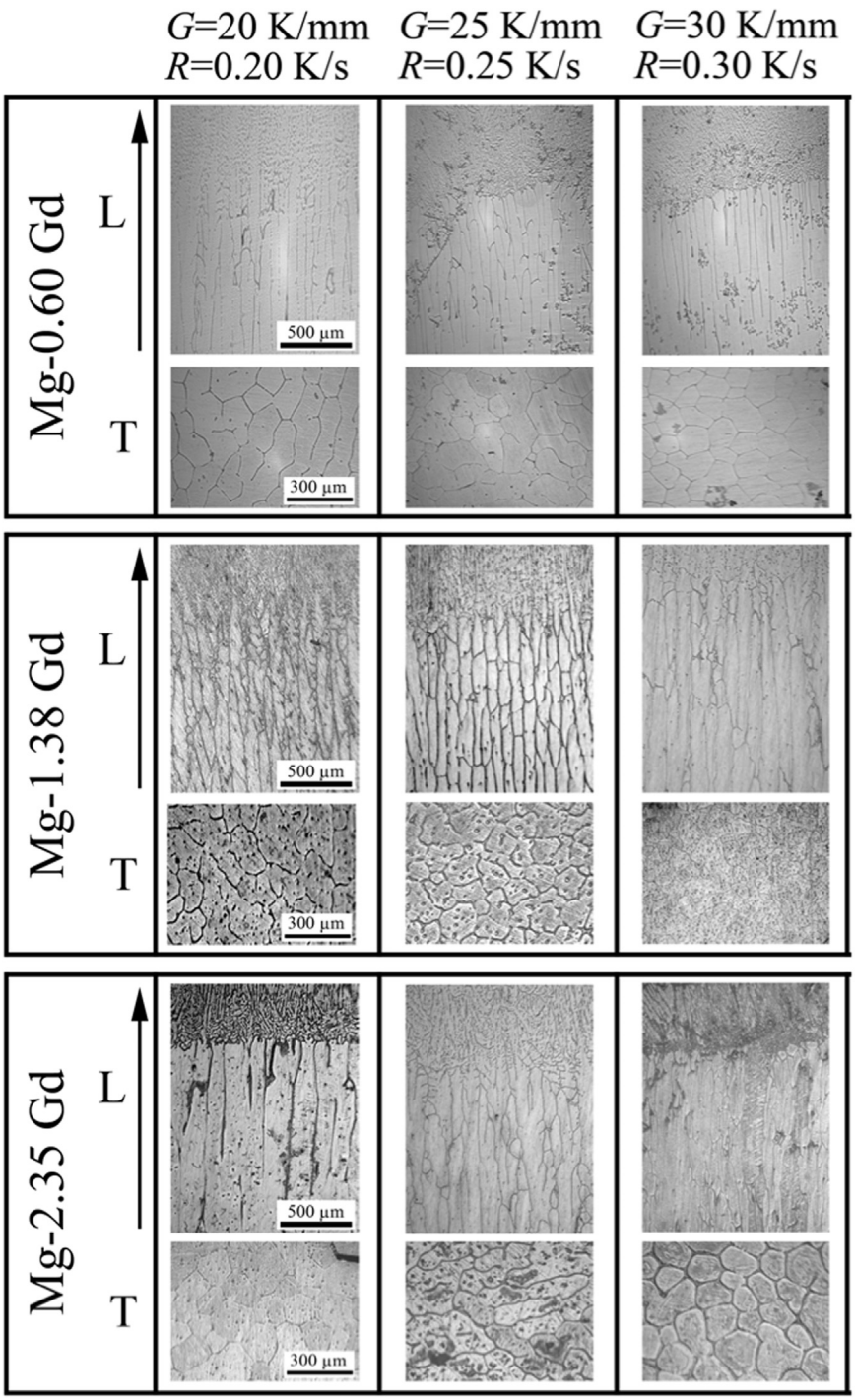

Fig. 2. OM images of directionally solidified Mg-Gd experimental alloys at $V=10$ μm/s under different temperature gradients. L and T represent the longitudinal and the transverse section of samples, respectively.

3. Results

3.1. Directional solidification microstructures

Fig. 1 and Fig. 2 show OM microstructures of the longitudinal and transversal section of directionally solidified Mg-Gd experimental alloys under the constant temperature gradient of 30 K/mm at different growth rates and at the constant growth rate of 10 μm/s under different temperature gradients, respectively. A typical cellular structure was observed in all experimental alloys. The cellular microstructures became finer with increasing the growth rate. It is worth nothing that a typical cellular structure with coarse trunks along the longitudinal section and a regular cellular structure on the transversal section were exhibited when the growth rate is less than 10 μm/s. When the growth rate is close to 100 μm/s, however, remarkable finer trunks along the longitudinal section and a mixed structure of dot-shape and strip-shape on the transversal section were observed. Further increasing the growth rate up to 200 μm/s, a finer cellular structure along the longitudinal section and a smooth cellular structure on the transversal section were observed. In addition, the width of the intercellular groove increases with increasing the growth rate and thereby the corresponding tip radii of cells decrease. Similar trends were also found, as shown in Fig. 2. The microstructures became finer when the temperature gradient increases from 20 K/mm to 30 K/mm at the given growth rate and solute content. Moreover, no significant effect of the solute content on the microstructural morphology was observed, although the cellular spacing (λ) increases with increasing the solute content at the given G and V.

3.2. Effect of the solidification parameters (G, V, R, C_0) on the cellular spacing

The measured cellular spacing (λ) of the Mg-Gd alloys are given in Table 2. The variation of cellular spacing (λ) as a function of the growth rates (V) is shown in Fig. 3a. A family of straight lines was obtained. The mathematical relationship between λ and V by a linear regression analysis for each composition can be, therefore, described as:

$$\lambda = k_1 V^{-a} \tag{2}$$

The values of the exponent (a) are close to 0.26, 0.26 and 0.28 for Mg-0.60 Gd, Mg-1.38 Gd and Mg-2.35 Gd, respectively, which are in good agreement with the values of 0.25, 0.23, 0.27, 0.25, 0.26 and 0.24 obtained by Yang et al. [16] for Cu-Mn, Lapin et al. [17] for Ni-Al-Cr-Fe, Kloosterman and Hosson [18] for TiN, Kaya et al. [19] for Al-Li and Gündüz et al. [20] for Al-Ti alloy, respectively. Furthermore, these exponent values are very close to the value of 0.25 predicted by Hunt [21], Kurz and Fisher [22], and Trivedi [23] theoretical models for cellular spacing.

The variations of λ values obtained from Mg-Gd alloys with G at the constant V (10 μm/s) are shown in Fig. 3b and Table 2. Again, a family of straight lines was observed with one line corresponding to one C_0. A linear regression analysis gives a proportionality equation as:

$$\lambda = k_2 G^{-b} \tag{3}$$

The values of exponent (b) are equal to 0.44, 0.31 and 0.71 for Mg-0.60 Gd, Mg-1.38 Gd and Mg-2.35 Gd, respectively, which are also in good agreement with the values of 0.32, 0.52 and 0.57, 0.72, and 0.32-0.71 obtained by Klaren et al. [24] for Pb-Sn, Tunca and

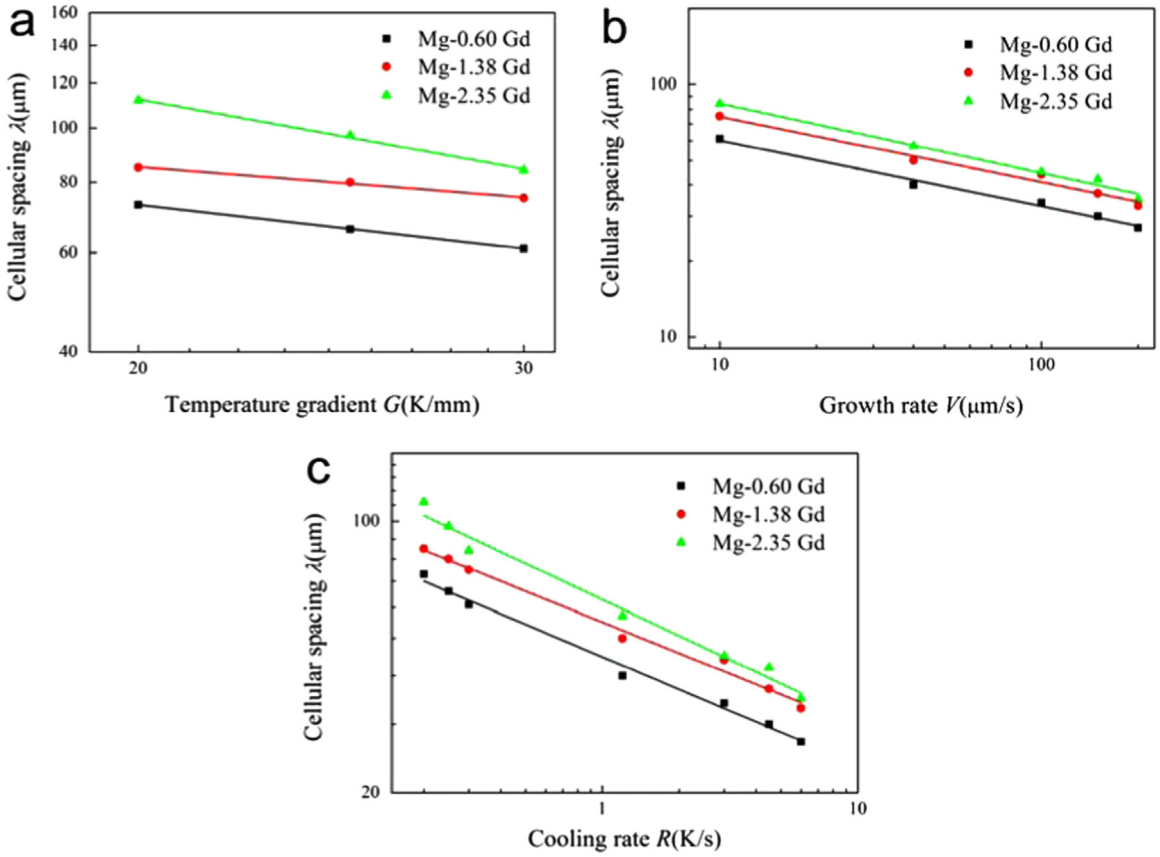

Fig. 3. (a) Variations of cellular spacing (λ) with growth rates (V) at the constant temperature gradient (G) (30 K/mm) for different Mg-Gd alloys; (b) variations of cellular spacing (λ) with temperature gradients (G) at the constant growth rate (V) (10 μm/s) for different Mg-Gd alloys; (c) variations of cellular spacing (λ) with cooling rates (R) for different Mg-Gd alloys.

Smith [25] for Zn-Al, Jacobi and Schwerdtfeger [26] by Fe-C-Mn, Çadırlı and Gündüz [27] for Pn-Sn alloys, respectively.

Fig. 3c shows the λ values obtained from Mg-Gd alloys as a function of the cooling rates (R). Clearly, the variations of λ versus R plot are essentially linear on the logarithmic scale. A linear regression analysis gives a proportionality equation as:

$$\lambda = k_3 G^{-c} \quad (4)$$

the values of the exponent (c) are equal to 0.28, 0.27 and 0.31 for Mg-0.60 Gd, Mg-1.38 Gd and Mg-2.35 Gd, respectively, which are in good agreement with the values of 0.55, 0.31, 0.33 and 0.29-0.40 obtained by Rocha et al. [28] for Sn-Pb, Kermanpur et al. [29] for Ni base superalloy (IN738LC), Trivedi et al. [30] for SCN-salol and Çadırlı and Gündüz [27] for Pb-Sn alloys, respectively.

As can be seen from Table 2 and Fig. 3a–c, the λ values obtained from Mg-Gd alloys increase with increasing Gd content under the same solidification parameters, G and V. This result is in good agreement with the theoretical models (Hunt model [21], Kurz and Fisher model [22], Trivedi model [23]). Furthermore, the influence of Gd content on the exponent (b) values of the temperature gradient is greater than the exponent (a) values of the growth rate and the exponent (c) values of the cooling rate.

3.3. Mechanical properties

Fig. 4 shows the results of ultimate tensile strength (σ_b) as a function of the cellular spacing λ. The classical Hall-Petch type equations are proposed to fit the experimental data [31]. Clearly, σ_b increases with decreasing λ. The relationships between σ_b and λ are given in Table 3.

Fig. 5 shows the variation of the ultimate tensile strength as a function of the cooling rates (R). As expected, increasing cooling rates (R) leads to an increase of the ultimate tensile strength. Through a linear regression analysis, the relationships between the ultimate tensile strength and the cooling rate are given in Table 3. The exponent values are close to 0.29, 0.30 and 0.32 for Mg-0.60 Gd, Mg-1.38 Gd and Mg-2.35 Gd alloys, respectively. It should be noted that the exponent values (0.29, 0.30 and 0.32) in the present work are different from the values of 0.55, 0.08 and 0.10 obtained by Ares et al. [32] for Zn-Al alloy and Çadırlı [33] for Al-Cu alloys, respectively, indicating that there is a slight variation of exponent values dependent on the particular alloy system and the alloy composition used.

Table 3
The relationships between ultimate tensile strength, cooling rate and cellular spacing for Mg-Gd alloys.

Alloys	Relationships	Correlation coefficient (r)
Mg-0.60 Gd	$\sigma_b = -104.13 + 1347.77\lambda^{-0.5}$	−0.986
	$\sigma_b = 93.41R^{0.29}$	0.997
Mg-1.38 Gd	$\sigma_b = -121.57 + 1674.28\lambda^{-0.5}$	−0.988
	$\sigma_b = 99.68R^{0.30}$	0.997
Mg-2.35 Gd	$\sigma_b = -110.76 + 1754.20\lambda^{-0.5}$	−0.985
	$\sigma_b = 105.34R^{0.32}$	0.995

4. Discussion

4.1. The formation of cellular structures

A typical cellular structure was observed, as shown in Fig. 1 and Fig. 2. The formation of cellular structures can be interpreted using

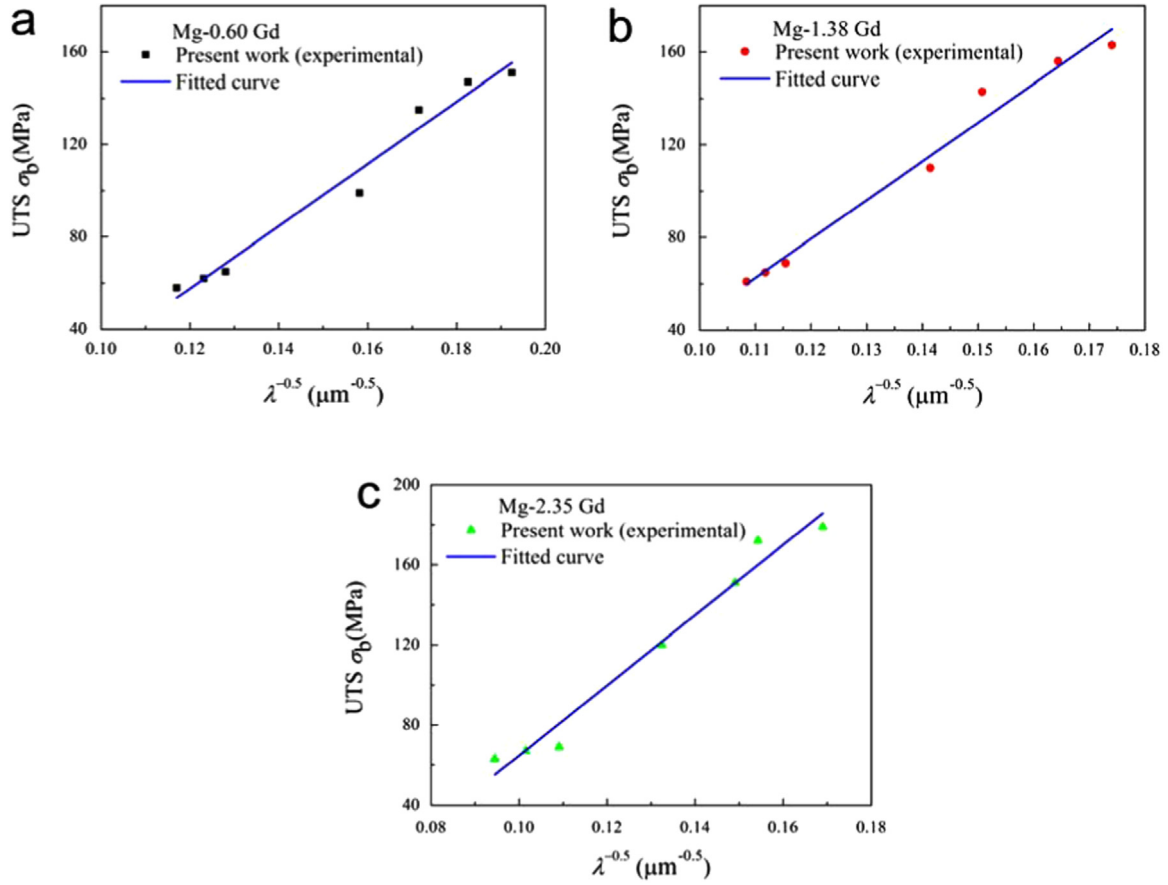

Fig. 4. Ultimate tensile strength as a function of the cellular spacing (λ) in different Mg-Gd alloys. (a) Mg-0.60 Gd alloy; (b) Mg-1.38 Gd alloy and (c) Mg-2.35 Gd alloy.

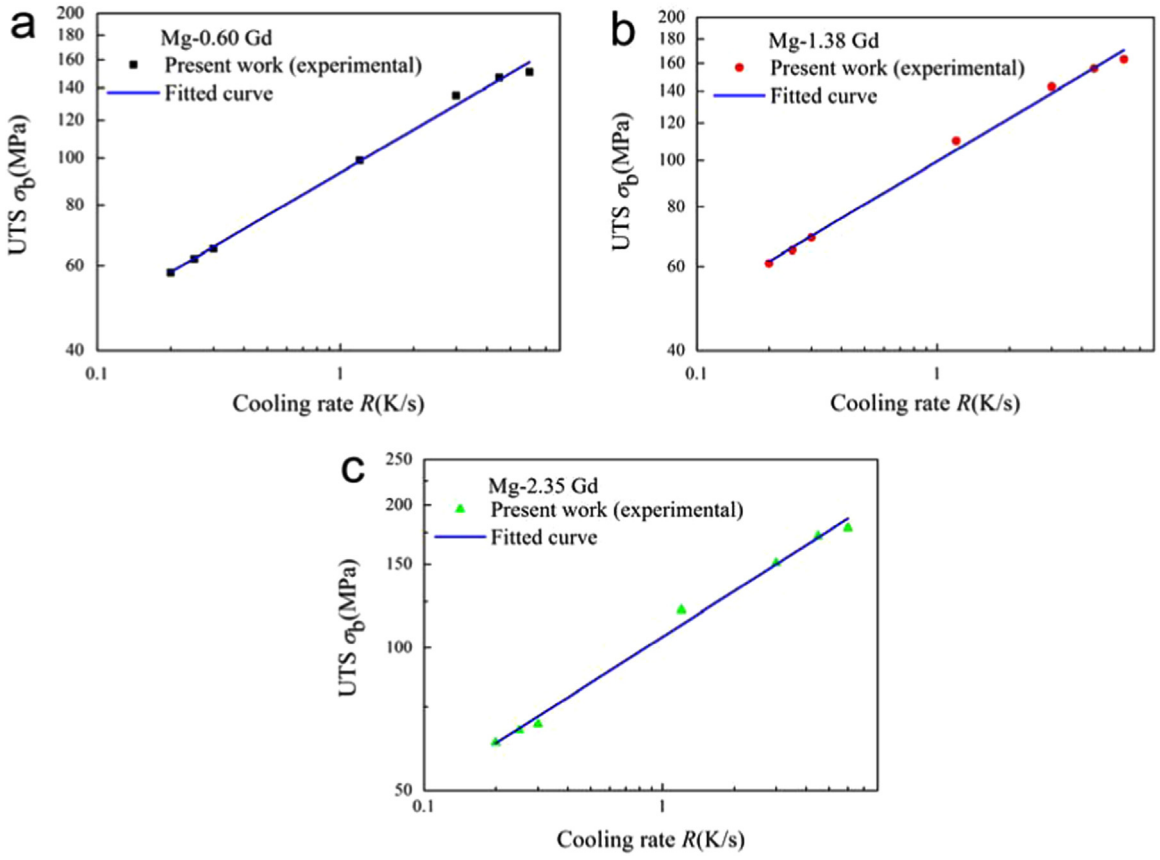

Fig. 5. The variations of the ultimate tensile strength as a function of the cooling rates (R) in different Mg-Gd alloys. (a) Mg-0.60 Gd alloy; (b) Mg-1.38 Gd alloy and (c) Mg-2.35 Gd alloy.

Table 4
Thermophysical parameters of Mg-Gd alloys.

Alloys	Liquidus slope m, (K/wt%)	Distribution coefficient k	Diffusion coefficient $D \times 10^{-9}$, m^2/s	Gibbs-Thomson coefficient $\Gamma \times 10^{-7}$, m K
Mg-0.60 Gd	−1.2171[a]	0.0916[a]	1.112 [37]	1.1 [37]
Mg-1.38 Gd	−1.2714[a]	0.0993[a]	1.233 [37]	1.1 [37]
Mg-2.35 Gd	−1.3353[a]	0.1011[a]	1.347 [37]	1.1 [37]

[a] The data are calculated using Thermo-Calc software.

the dendrite growth theory proposed by Kurz-Fisher [22] and Hunt and Lu [34,35]. According to the dendrite growth theory of Kurz-Fisher [22], the approximate criterion growth rate (V_{tr}) for cell/dendrite transition can be expressed as:

$$V_{tr} = \frac{GD}{\Delta T_0 k} = \frac{GD}{mc_0(k-1)} \quad (5)$$

where G is the temperature gradient in the liquid, D is the diffusion coefficient of solute atom in the liquid, ΔT_0 is the temperature interval between the liquidus and the solidus, k is the distribution coefficient, m is the liquidus slope and C_0 is the initial composition of the solidifying alloy. Using the physical parameters given in Table 4, the V_{tr} of Mg-0.60 Gd, Mg-1.38 Gd and Mg-2.35 Gd alloys can be evaluated to be 50.3 μm/s, 23.4 μm/s and 13.1 μm/s at the constant temperature gradient of 30 K/mm, respectively. Clearly, the experimental solidification microstructures are still in the range of the cellular structure according to the theoretical criterion growth rate for cell/dendrite transition, which can be used to

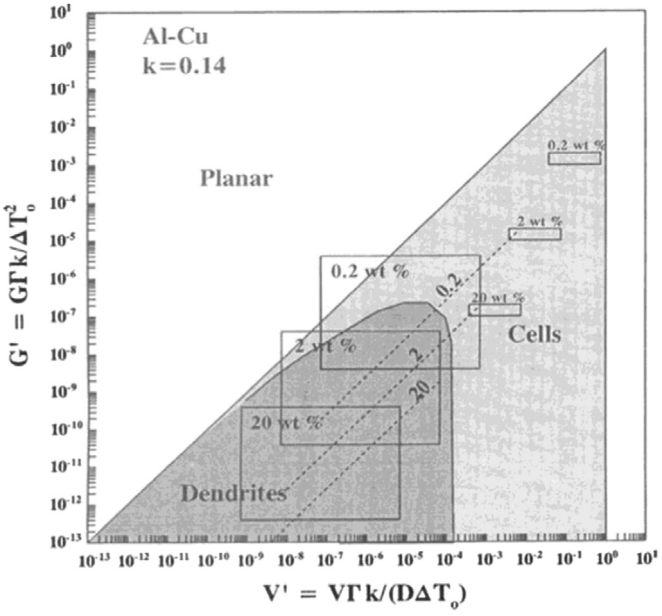

Fig. 6. The microstructure/processing map in the dimensionless G'-V' domain for Al-Cu alloy [36]. The triangular-shaped region indicates that cells and dendrite may form.

interpret the absence of dendrite structure with changing the growth rate. It should be noted that the Kurz-Fisher model [22] does not take the effects of the interfacial energy and the solidification behavior of the specific alloy into account. Instead, taking the interfacial energy into consideration, Hunt and Lu [34,35]

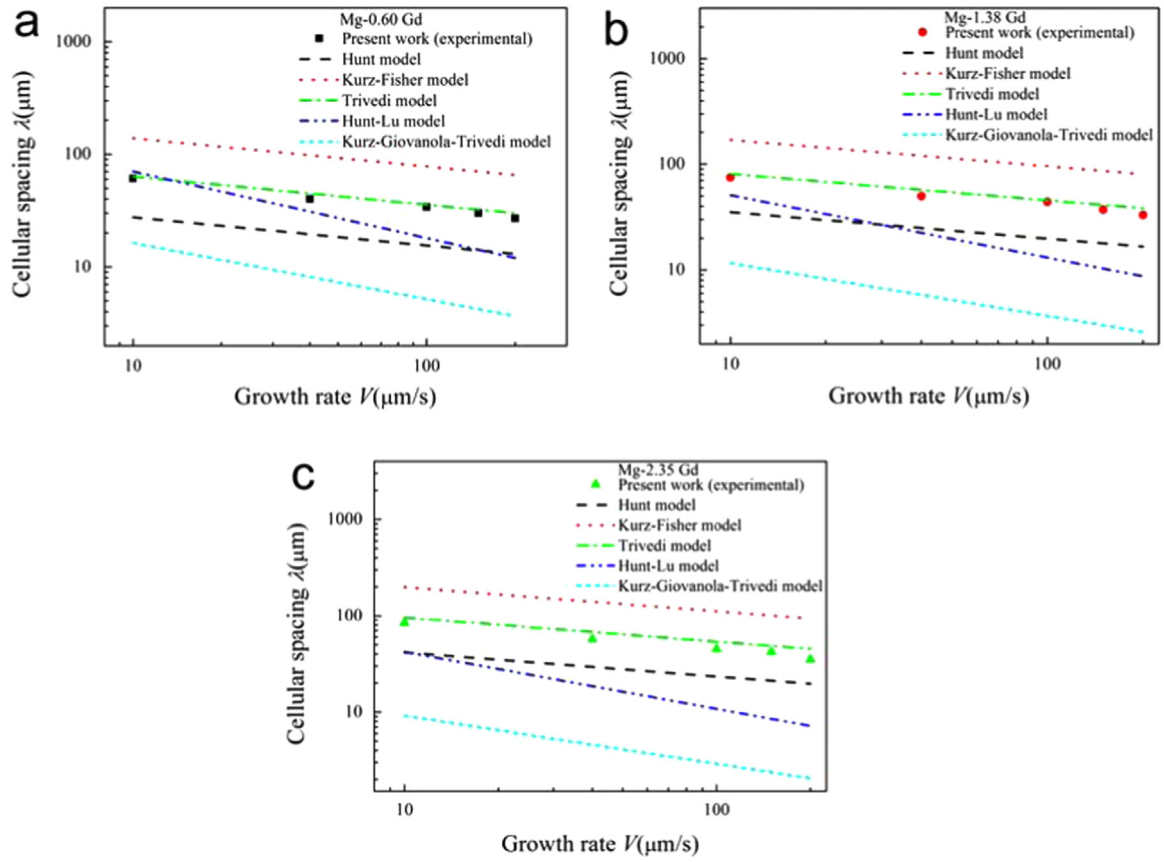

Fig. 7. The comparison of cellular spacing (λ) obtained from different Mg-Gd alloys with the theoretical models and numerical models. (a) Mg-0.60 Gd alloy; (b) Mg-1.38 Gd alloy and (c) Mg-2.35 Gd alloy.

proposed the microstructure/processing map in the dimensionless temperature gradient G'($G' = G\Gamma k/\Delta T^2$) and growth rate V'($V' = V\Gamma k/D\Delta T_0$, $\Delta T_0 = mc_0(k-1)/k$) domain for Al-Cu alloy, as shown in Fig. 6 [36]. Clearly, the solute content has a significant effect on the morphology evolution. A smaller content results in a smaller corresponding scope of dendrite and an easier way to obtain a high speed cellular structure. Considering the high solubility of Gd (23.5 wt%) in Mg [5,6], the solute (Gd) content in this work is relatively less and thus only cellular structures were observed.

4.2. The comparison of the experimental results with the theoretical models

The comparison of the λ values obtained from Mg-Gd alloys with the calculated λ values using the theoretical models (Hunt model [21], Kurz and Fisher model [22], Trivedi model [23]) and numerical models (Hunt and Lu model [37] and Kurz et al. model [38,39]) is shown in Fig. 7. The calculated λ values by Kurz-Fisher model for all compositions are higher than the experimental λ values. In contrast, the calculated λ values by Hunt model for all compositions are fairly lower than the experimental λ values. More interestingly, the experimental λ values are in good agreement with the calculated λ values by Trivedi model, indicating that the Trivedi model can be used to predict the cellular spacing of directionally solidified Mg-Gd alloys with a reasonable accuracy. Furthermore, the comparison of the λ values obtained from Mg-Gd alloys with the numerical models for Mg-0.60 Gd, Mg-1.38 Gd and Mg-2.35 Gd is also shown in Fig. 7a-c, respectively. The calculated λ values by Hunt-Lu model and Kurz-Giovanola-Trivedi model are fairly lower than the experimental λ values, which may be due to the high growth rate exponent values (0.59 and 0.50) for the numerical models.

4.3. Strengthening mechanism

The ultimate tensile strength (σ_b) increases with decreasing cellular spacing (λ). It has been reported [31,32,40,41] that the direction solidification microstructure has a significant effect on mechanical properties. Different slopes obtained from the relationships between ultimate tensile strength and the inter-branch spacing have been reported by Spinelli [31], which may be caused by different microstructure features. It is worth nothing that, in this paper, no significant change of the slopes was observed. This is due to the fact that a typical cellular structure was observed, as shown in Fig. 1 and Fig. 2. The main reason for improving the ultimate tensile strength can be mainly attributed to the smaller cellular spacing (λ) duo to the increase of solidification parameters, G and V.

Furthermore, increasing cooling rate (R) also leads to an increase of the ultimate tensile strength, which can be attributed to the fact that with increasing cooling rate, the mean size of the second phase decreases [42,43]. It should be noted that the direction solidification condition in this investigation is non-equilibrium. Although the solubility of Gd in Mg is quite high, the solute Gd segregates into grain boundaries and thereby forms second phase particles (e,g, Mg_5Gd, Mg_3Gd) along grain boundaries during solidification. During the solidification process of cellular structure alloys, the solid–liquid interface consists of families of finger-like projections (cells) moving in unison while sweeping ahead of the solute-rich liquid. The liquid at the interface contains a high concentration of solute elements, and it solidified, forming

brittle and coarse phases along the grain boundaries, which serve as regions for the crack initiation or propagation during the tensile test [40]. Thus, an increase in cooling rate results in a decrease in crack source, and finally leads to a finer second phase. Moreover, as shown Fig. 4 and Fig. 5, the ultimate tensile strength became higher as the solute Gd content increases from 0.60 to 2.35 at the same conditions, indicating that a certain amount of Gd are dissolved in α(Mg), which would also improve the ultimate tensile strength.

5. Conclusions

Mg-xGd (x=0.60, 1.38, and 2.35) alloys were directionally solidified under various solidification conditions, and their microstructural evolution was observed from the longitudinal and transverse sections of specimens. The influence of cellular spacing dependent on solidification parameter (G, V, C_0) on the mechanical properties was also discussed. The main conclusions can be drawn:

(1) A typical cellular microstructures was observed in directionally solidified Mg-xGd (x=0.60, 1.38, and 2.35) alloys under a constant G (30 K/mm) at a wide range of V (10–200 μm/s) and with a constant V (10 μm/s) at a wide range of G (20–30 K/mm), which may be attributed to the combined effects of the lower solute content and the higher interfacial tension.
(2) The cellular spacing λ decreases with increasing solidification parameters, G and V. The values of cellular spacing calculated by Kurz-Fisher model and Hunt model obviously diverged from the measured results, while the measured results are in good agreement with the values calculated by Trivedi model. The Trivedi model could be used to predict the cellular spacing of Mg-Gd alloys under G=20–30 K/mm and V=10–200 μm/s with a reasonable accuracy.
(3) The cellular spacing λ increases with increasing Gd content for the given solidification parameters, G and V, which is in good agreement with the theoretical models.
(4) The direction solidification microstructure structure has a significant effect on mechanical properties. The ultimate tensile strength decreases with increasing cellular spacing, but it increases with increasing cooling rate, which may be attributed to the smaller cellular spacing and the finer size of second phase.

Acknowledgements

Financial supports by the National Natural Science Foundation of China (Grant nos. 51227001 and 51420105005) and the Research Fund of the State Key Laboratory of Solidification Processing (NWPU), China (Grant no. 138-QP-2015) are gratefully acknowledged.

References

[1] S. Schumann, H. Friedrich, Current and future use of magnesium in the automobile industry, Mater. Sci. Forum 419–422 (2003) 51–56.
[2] B.L. Mordike, T. Ebert, Magnesium properties-applications-potential, Mater. Sci. Eng. A 302 (1) (2001) 37–45.
[3] Z. Zhang, A. Couture, Alan Luo, An investigation of the properties of Mg-Zn-Al alloys, Scr. Mater. 39 (1) (1998) 45–53.
[4] B.H. Kim, S.W. Lee, Y.H. Park, I.M. Park, The microstructure, tensile properties, and creep behavior of AZ91, AS52 and TAS652 alloy, J. Alloy. Compd. 493 (1–2) (2010) 502–506.
[5] I.A. Anyanwu, S. Kamado, Y. Kojima, Aging characteristics and high temperature tensile properties of Mg-Gd-Y-Zr alloys, Mater. Trans. 42 (7) (2001) 1206–1211.
[6] L. Gao, R.S. Chen, E.H. Han, Effects of rare-earth elements Gd and Y on the solid solution strengthening of Mg alloys, J. Alloy. Compd. 481 (1–2) (2009) 379–384.
[7] M. Nishijima, K. Hiraga, Structural changes of precipitates in an Mg-5 at% Gd alloy studied by transmission electron microscopy, Mater. Trans. 48 (1) (2007) 10–15.
[8] J.F. Nie, K. Oh-ishi, X. Gao, K. Hono, Solute segregation and precipitation in a creep-resistant Mg–Gd–Zn alloy, Acta Mater. 56 (20) (2008) 6061–6076.
[9] T. Honma, T. Ohkubo, S. Kamado, K. Hono, Effect of Zn additions on the age-hardening of Mg–2.0Gd–1.2Y–0.2Zr alloys, Acta Mater. 55 (12) (2007) 4137–4150.
[10] S.J. Liu, G.Y. Yang, S.F. Luo, W.Q. Jie, Microstructure evolution during heat treatment and mechanical properties of Mg–2.49Nd–1.82Gd–0.19Zn–0.4Zr cast alloy, Mater. Charact. 107 (2015) 334–342.
[11] J. Wang, J. Meng, D.P. Zhang, D.:X. Tang, Effect of Y for enhanced age hardening response and mechanical properties of Mg–Gd–Y–Zr alloys, Mater. Sci. Eng. A 456 (1–2) (2007) 78–84.
[12] Q.M. Peng, X.L. Hou, L.D. Wang, Y.M. Wu, Z.Y. Cao, L.M. Wang, Microstructure and mechanical properties of high performance Mg–Gd based alloys, Mater. Des. 30 (2) (2009) 292–296.
[13] S.M. He, X.Q. Zeng, L.M. Peng, X. Gao, J.F. Nie, W.J. Ding, Microstructure and strengthening mechanism of high strength Mg–10Gd–2Y–0.5Zr alloy, J. Alloys Compd. 427 (1–2) (2007) 316–323.
[14] M. Paliwal, I.H. Jung, The evolution of the growth morphology in Mg–Al alloys depending on the cooling rate during solidification, Acta Mater. 61 (13) (2013) 4848–4860.
[15] S.J. Liu, G.Y. Yang, W.Q. Jie, Microstructure, microsegregation, and mechanical properties of directional solidified Mg–3.0Nd–1.5Gd alloy, Acta Met. Sin. 27 (6) (2014) 1134–1143.
[16] S. Yang, W.:D. Huang, X. Lin, Y.P. Su, Y.H. Zhou, On cellular spacing selection of Cu-Mn alloy under ultra-high temperature gradient and rapid solidification condition, Scr. Mater. 42 (6) (2000) 543–548.
[17] J. Lapin, A. Klimová, R. Velisek, M. Kursa, Directional solidification of Ni-Al-Cr-Fe alloy, Scr. Mater. 37 (1) (1997) 85–91.
[18] A.B. Kloosterman, J.TH.M. de Hosson, Cellular growth and dislocation structures in laser-nitrided titanium, J. Mater. Sci. 32 (23) (1997) 6201–6205.
[19] H. Kaya, E. Çadırlı, M. Gündüz, Directional cellular growth of Al-2 wt% Li bulk samples, Appl. Phys. A. 94 (1) (2008) 155–165.
[20] M. Gündüz, H. Kaya, E. Çadırlı, N. Maraşlı, K. Keşlioğlu, B. Saatçi, Effect of solidification processing parameters on the cellular spacings in the Al–0.1 wt% Ti and Al–0.5 wt% Ti alloys, J. Alloy. Compd. 439 (1–2) (2007) 114–127.
[21] J.D. Hunt, Solidification and Casting of Metals, The Metal Society, London 1979, pp. 3–9.
[22] W. Kurz, D.J. Fisher, Dendrite growth at the limit of stability: tip radius and spacing, Acta Met. 29 (1) (1981) 11–20.
[23] R. Trivedi, Interdendritic spacing: Part II. A comparison of theory and experiment, Metall. Mater. Trans. A 15 (6) (1984) 977–982.
[24] C.M. Klaren, J.D. Verhoeven., R. Trivedi, Primary dendrite spacing of lead dendrites in Pb-Sn and Pb-Au Alloys, Metall. Trans. A 11 (11) (1980) 1853–1861.
[25] N. Tunca, R.W. Smith, Variation of dendrite arm spacing in Al-rich Zn-Al off-eutectic alloys, J. Mater. Sci. 23 (1) (1988) 111–120.
[26] H. Jacobi, K. Schwerdtfeger, Dendrite morphology of steady state unidirectionnally solidified steel, Metall. Trans. A 7 (6) (1976) 811–820.
[27] E. Çadırlı, M. Gündüz., The directional solidification of Pb-Sn Alloys, J. Mater. Sci. 35 (15) (2000) 3837–3848.
[28] O.L. Rocha, C.A. Siqueira, A. Garcia, Cellular/dendritic transition during unsteady-state unidirectional solidification of Sn–Pb alloys, Mater. Sci. Eng. A 347 (1–2) (2003) 59–69.
[29] A. Kermanpur, N. Varahraam, E. Engilehei, M. Mohammadzadeh, P. Davami, Directional solidification of Ni base superalloy IN738LC to improve creep properties, Mater. Sci. Technol. 16 (5) (2000) 579–586.
[30] R. Trivedi, Y.:X. Shen, S. Liu, Cellular-to-dendritic transition during the directional solidification of binary alloys, Metall. Mater. Trans. A 34 (2) (2003) 395–401.
[31] J.E. Spinelli, A. Garcia, Microstructural development and mechanical properties of hypereutectic Sn–Cu solderalloys, Mater. Sci. Eng. A 568 (2013) 195–201.
[32] A.E. Ares, C.E. Schvezov, The effect of structure on tensile properties of directionally solidified Zn-based alloys, J. Cryst. Growth 318 (1) (2011) 59–65.
[33] E. Çadırlı., Effect of solidification parameters on mechanical properties of directionally solidified Al-rich Al-Cu alloys, Met. Mater. Int. 19 (3) (2013) 411–422.
[34] S.Z. Lu, J.D. Hunt, A numerical analysis of dendritic and cellular array growth the spacing adjustment mechanisms, J. Cryst. Growth 123 (1) (1992) 17–34.
[35] J.D. Hunt, S.Z. Lu, Numerical modelling of cellular and dendritic array growth spacing and structure predictions, Mater. Sci. Eng. A 173 (1) (1993) 79–83.
[36] J.D. Hunt, S.Z. Lu, Numerical modeling of cellular/dendritic array growth: spacing and structure predictions, Metall. Mater. Trans. A 27 (3) (1996) 611–623.
[37] W. Kurz, D.J. Fisher, Fundanmentals of Solidification, Trans Tech Publications, London 1998, pp. 11–30.
[38] W. Kurz, B. Giovanola, R. Trivedi, Theory of microstructural development during rapid solidification, Acta Met. 34 (5) (1986) 823–830.
[39] W. Kurz, B. Giovanola, R. Trivedi., Microsegregation in rapidly solidified Ag-

15 wt% Cu, J. Cryst. Growth 91 (1–2) (1988) 123–125.
[40] J. Hofweber, N.F. Fiore, Effects of solidification substructure on the mechanical properties of a nickel base superalloy, Mater. Sci. Eng. A 27 (2) (1977) 157–162.
[41] W.R. Osório, C.A. Santos, J.M.V. Quaresma, A. Garcia, Mechanical properties as a function of thermal parameters and microstructure of Zn–Al castings, J. Mater. Process. Technol. 143–144 (2003) 703–709.
[42] X.W. Zheng, A. Luo, C. Zhang, J. Dong, R.A. Waldo, Directional solidification and microsegregation in a magnesium-aluminum-calcium alloy, Metall. Mater. Trans. A 43 (9) (2012) 3239–3248.
[43] C. Zhang, D. Ma, K.S. Wu, H.B. Cao, G.P. Cao, S. Kou, Y.A. Chang, X.Y. Yan, Microstructure and microsegregation in directionally solidified Mg–4Al alloy, Intermetallics 15 (10) (2007) 1395–1400.